

# Shadows of a Non-Commutative Black Hole under the Influence of a Magnetized Plasma

Mrinmoy M. Gohain<sup>1,2,\*</sup>, Kalyan Bhuyan<sup>1,3,†</sup> and Paragjyoti Chutia<sup>1,2,‡</sup>

<sup>1</sup>Department of Physics, Dibrugarh University, Dibrugarh  
Assam, India, 786004

<sup>2</sup>Department of Physics, DHSK College, Dibrugarh  
Assam, India, 786001

<sup>3</sup>Theoretical Physics Division, Centre for Atmospheric Studies,  
Dibrugarh University, Dibrugarh, Assam, India 786004

We investigate the properties of the shadow cast by a black hole in a non-commutative spacetime surrounded by a plasma medium. Black holes in a plasma environment can exhibit complex interactions that profoundly affect their shadow properties. In specific terms, we consider a special type of plasma medium motivated from the interactions among axions, photons and plasma excitations, or commonly termed as axion-plasmon in the presence of a magnetic field. We have studied the effect of these plasma parameters and the non-commutative parameter on the shadow properties by focusing particularly the photon sphere radius, angular shadow and the shadow observed from the observer's perspective. For this we have considered two different forms of plasma *viz.* homogeneous and inhomogeneous plasma. In this work we have presented the parameter dependence of these BH shadow properties.

## I. INTRODUCTION

Black holes (BH) are regions of extreme curvature in spacetime predicted by general relativity (GR), are one of the most fascinating entities in the universe. A key motivation for studying BHs is to test GR in the strong-field regime and to understand the fate of collapsing massive stars. Furthermore, BHs play an important role in the evolution of galaxies, often by residing at the galactic centers and by influencing the dynamics of surrounding stars and gas.

Recent work on BHs explores various aspects, including the resolution of singular points of infinite density at the center of classical BHs. One of such approach deals with non-commutative geometry of spacetime, which introduces a fundamental "fuzziness" to spacetime at extremely small scales [1–3]. This is termed loosely as "smearing of mass". The smearing of mass, inspired by non-commutative geometry, helps avoid singularities in black hole solutions by preventing the gravitational collapse of matter into an infinitely dense point. Instead of a point-like singularity, the mass distribution becomes spread out over a finite region, often modeled by a Gaussian or Lorentzian distribution [1]. Non-commutative geometry introduces an intrinsic uncertainty in the localization of points in spacetime, which fundamentally suggests how matter and

energy are may be distributed, especially in situations with strong gravitational fields. As a result, singularities, which arise from assuming point-like matter distributions, may be avoided by considering non-local matter distributions. This concept of smearing of the mass distribution plays a significant role in the curvature of spacetime in the manner that, classically, in a BH, the curvature becomes infinite at the singularity but with a smeared mass distribution, the spacetime curvature stays finite even at the centre of the BH. This produces a regular BH solution. Quantitatively, the extent of the smeared region is parameterized by the non-commutativity parameter, usually represented as  $\sqrt{\theta}$ , which intriduces an intrinsic length scale below which the classical definition of a point like object becomes redundant. The basis for the application of non-commutative geometry to black holes is the idea that spacetime coordinates cannot be measured with infinite accuracy. The amount of energy needed for such accurate measurements would necessarily change the geometry at these scales, introducing an inherent precision in coordinate measurements. This is somewhat analogous to the Heisenberg uncertainty principle in quantum mechanics. Some important works carried out recently using non-commutative spacetime includes the work of Toghrai et al [4] where they studied the non-commutative formalism of a Schwarzschild black hole and some of its physical features. Bhar et al [5] investigated the thermodynamical properties, shadows, quasinormal modes of the noncommutative BH in the framework of de Rham-Gabadadze-Tolley like massive gravity. Some other works can be found in Refs. [6–16].

---

\* mrinmoygohain19@gmail.com

† kalyanbhuyan@dibru.ac.in

‡ paragjyotic@gmail.com

The surroundings of a galactic BH can contain matter in the form of plasma. This is because, as matter accretes onto a black hole, it is heated by gravity and friction to extremely high temperatures in a hot accretion disk. The heat ionizes the accreting matter, thus forming a plasma that emits energy over the entire electromagnetic spectrum, and can be an interesting probe from the observational point of view. The plasma environment can also be a useful ingredient in a wide range of astrophysical processes, including the production of relativistic jets from the black hole poles and the production of strong magnetic fields. There have been many works dedicated to the effect of plasma on the optical properties of BHs, for instance in a work by Atamurotov et al, [17], they studied the motion of photons around a Kerr black hole in a plasma with a radial power-law parameterization of density and found that the black hole shadow size and shape are dependent on the plasma parameter, spin, and inclination angle, while in a Schwarzschild BH, the photon sphere remains unchanged, but the shadow size is reduced by refraction, and the highest energy emission rate gets reduced in the presence of plasma. In another work by Perlick et al, [18] they studied the effect of a non-magnetized plasma on the shadows in spherically symmetric spacetimes, and they derived general formulas which they used in studying Schwarzschild BHs and Ellis wormholes, including free-fall plasma cases and discussed the observational perspectives on the shadows of supermassive BHs. Abdujabbarov et al [19] discussed the shadow of a rotating BH with quintessential energy in both vacuum and plasma and found that in vacuum the quintessential field enlarges the radius of the shadow and diminishes its distortion, whereas in a plasma medium, the shape of the shadow is depends crucially on the plasma parameters, spin, and the quintessential field. There are several other works dealing with the effect of plasma on BH properties and can be found in [20–23] etc.

Furthermore, plasma around a black hole may also couple to theoretical particles like axions (which were proposed to solve the strong CP problem in particle physics) through superradiance, draining energy and angular momentum from spin of black holes [24, 25]. Superradiating would produce an axion cloud dense near the black hole. Plasma can have a significant role in this phenomenon as well as in the development of the axion cloud. Although not a standard terminology, the "axion-plasmon" terminology reflects the interesting interaction among axions, photons and plasma excitations near the BH environment. Plasma influences, like screening electric charges and modifications of the photon propagation [26] can affect the interaction between

axions and the electromagnetic field and may produce observable signatures [27–29]. Analysis of these couplings has the potential to add valuable perspectives to both axion physics as well as plasmas in a strong gravitational field. Some of the important works based on the effect of axion-plasmon on the optical properties of BHs include the works of Atamurotov et al [30] where they studied the effect of axion-plasmon coupling on the null trajectories around a Schwarzschild BH and how it affects the BH shadow, deflection angle and Einstein rings caused by radially infalling gas on the BH in the presence of a plasma medium. They found that these optical properties are influenced by the axion-plasmon coupling parameter. They also showed that the size of the BH shadow decreases with the increase in the axion-plasmon parameter if the observer's position lies sufficiently far away. Khodadi [31] investigated the shadow of a spinning BH within an axion-plasmon cloud and observed that axion-photon interaction affects the shadow size and shape. He found that with increasing value of axion-plasmon coupling, the size of the shadow increases for high-spinning BHs, whereas more massive axions shows small impact; in the non-rotating case, the shadow size diminishes, and the axion-plasmon cloud boosts energy emission for rotating BHs but seen to decrease as the rotation is slower. Pahlavon [32] studied the effect of a plasma medium on a Reissner Nördstrom BH where the effects of axion-plasmon coupling on the optical features of a charged BH is investigated, and they found that the photon geodesics, shadow radius, deflection angle, Einstein rings. It was shown that the shadow size decreases as charge increases, whereas its appearance varies with the plasma model in consideration, and it is maximum without plasma and minimum in the case of homogeneous plasma. Some other progress in the arena of BHs in a plasma environment over the recent years includes the work of Ali et al [33] where they studied deflection of light and shadow properties of a hairy BH under the effect of non-magnetic plasma. Rukkiyya and Sini [34] investigated strong lensing properties and shadows of a quantum Schwarzschild BH in the presence of a homogeneous plasma medium. Umarov et al [35] studied the optical properties under the influence of plasma medium around a Sen black hole, particularly on the shadow, weak lensing, and time delay properties. Alimova et al [36] investigated weak lensing and shadows in the framework of Kalb–Ramond gravity in Reissner–Nordström spacetime using uniform plasma, singular and non-singular isothermal spheres. Some other relevant works can be found in [37–42].

## II. PHOTON MOTION AROUND THE BH IN THE PRESENCE OF AXION-PLASMON

In this work, we want to explore the consequences of the optical properties of a non-commutative BH in a generalized electromagnetic theory which includes the axion-photon interaction in it [32, 43, 44]. As a result, one needs to introduce an extra term, that accounts for the axion-photon interaction. The Einstein-Maxwell action is given by

$$S = \int \left( \frac{R}{16\pi} - \frac{1}{4} F_{\mu\nu} F^{\mu\nu} \right) \sqrt{-g} d^4x + S_{\text{matter}}, \quad (1)$$

where

$$S_{\text{matter}} = \int \mathcal{L}_{\text{matter}} \sqrt{-g} d^4x, \quad (2)$$

with

$$\mathcal{L}_{\text{matter}} = \mathcal{L}_{\varphi} - A_{\mu} J_e^{\mu} + \mathcal{L}_{\text{int}}. \quad (3)$$

In our work, we shall assume that the surrounding plasma does not significantly impact on the overall curvature of spacetime. We are only interested in what role the plasma medium plays in determining the photon trajectories. The interaction between the electromagnetic field and the plasma can affect the energy shifts of the photons, which probably can dictate the optical properties around the BH. In the action given by Eq. (1) above,  $J_e^{\mu}$  represents the four-current associated with electrons, while  $F_{\mu\nu}$  is the electromagnetic field tensor, that embeds the electric and magnetic field components. The axion Lagrangian contribution is given by  $\mathcal{L}_{\varphi} = \nabla_{\mu} \varphi^* \nabla^{\mu} \varphi - m_{\varphi}^2 |\varphi|^2$ , which describes the dynamics of the axion field, including the kinetic and mass terms. The interaction term  $\mathcal{L}_{\text{int}} = -(g/4) \varepsilon^{\mu\nu\alpha\beta} F_{\alpha\beta} F_{\mu\nu}$  represents the interaction between axions and photons. This term, where  $g$  denotes the strength of the axion-photon coupling, describes how axions affect the electromagnetic field through a pseudoscalar interaction [32].

The static spherically symmetric spacetime metric for the Non-Commutative BH is

$$ds^2 = -f(r) dt^2 + \frac{1}{f(r)} dr^2 + r^2 (d\theta^2 + \sin^2 \theta d\phi^2), \quad (4)$$

where

$$f(r) = 1 - \frac{2M}{r} + \frac{8M\sqrt{\theta}}{\sqrt{\pi} r^2}.$$

Here,  $M$  and  $\theta$  are the mass and non-commutative parameter of the BH, respectively.

If we are interested in photon trajectories about a BH in the presence of axion-plasmon medium, the Hamiltonian can be defined as [45]

$$\mathcal{H}(x^{\alpha}, p_{\alpha}) = \frac{1}{2} [g^{\alpha\beta} p_{\alpha} p_{\beta} - (n^2 - 1)(p_{\beta} u^{\beta})^2], \quad (5)$$

Here, the spacetime coordinates, four-velocity and four-momentum of the photon are defined by  $x^{\alpha}$ ,  $u^{\beta}$  and  $p_{\alpha}$  respectively. Also,  $n$  is the refractive index of the plasma medium ( $n = \omega/k$ , with  $k$  as the wave number). The refractive index of the plasma medium in the framework with the axion-plasmon term is given by [43]

$$n^2 = 1 - \frac{\omega_p^2}{\omega^2} - \frac{f_0}{\gamma_0} \frac{\omega_p^2}{(\omega - k u_0)^2} - \frac{\Omega^4}{\omega^2 (\omega^2 - \omega_{\varphi}^2)} - \frac{f_0}{\gamma_0} \frac{\Omega^4}{(\omega - k u_0)^2 (\omega^2 - \omega_{\varphi}^2)}, \quad (6)$$

where

$$\omega_p^2(x^{\alpha}) = 4\pi e^2 N(x^{\alpha}) / m_e$$

is the plasma frequency in which  $e$ ,  $m_e$  and  $N$  denotes the electron charge, mass and number density of electrons. Here,  $\omega(x^{\alpha})$  is the photon frequency defined as  $\omega^2 = (p_{\beta} u^{\beta})^2$ ; the axion frequency is denoted by  $\omega_{\varphi}^2$ ; the axion-plasmon coupling parameter is given by  $\Omega = (g B_0 \omega_p)^{1/2}$  with  $B_0$  as the homogeneous magnetic field directed in the  $z$ -direction, where  $g$  represents the axion-photon coupling [43]<sup>1</sup>. Given the axial symmetry of the magnetic field and the spherically symmetric nature of the spacetime, we shall assume that the effects of strong curvature predominantly govern the particle dynamics, thereby dominating the influence of the magnetic field. The fraction of electron beam moving inside the plasma with velocity  $u_0$  is given by  $f_0$ , where  $\gamma_0$  is the associated Lorentz factor. As we are uncertain about the significance of the electron beam scenario in the vicinity of the BH, it will be convenient for us to set  $f_0 = 0$  for the sake of simplicity. Then, we can rewrite (6) as [17]

$$n^2(r) = 1 - \frac{\omega_p^2(r)}{\omega(r)^2} - \frac{\Omega^4}{\omega(r)^2 [\omega(r)^2 - \omega_{\varphi}^2]}, \\ = 1 - \frac{\omega_p^2(r)}{\omega(r)^2} \left( 1 + \frac{g^2 B_0^2}{\omega(r)^2 - \omega_{\varphi}^2} \right), \quad (7)$$

with

$$\omega(r) = \frac{\omega_0}{\sqrt{f(r)}}, \quad \omega_0 = \text{const}. \quad (8)$$

<sup>1</sup> Here,  $g$  should not be confused with the determinant of the metric tensor.

For the experimental requirements for axion-plasmon conversion, the plasma frequency scale must satisfy the inequality  $\omega_p^2 \gg \Omega^2$  (or equivalently,  $\omega_p \gg gB_0$ ). According to [18], the photon energy at spatial infinity is given by  $\omega(\infty) = \omega_0 = -p_t$ , and the lapse function is defined such that  $f(r) \rightarrow 1$  as  $r \rightarrow \infty$ . In addition, for distinguishing the BH shadow from the vacuum case, the plasma frequency must continue to be much smaller than the photon frequency, i.e.  $\omega_p^2 \ll \omega^2$ . Now, for light ray propagation in an axion-plasmon medium, the Hamiltonian can be recast in the following way: [45, 46]

$$\mathcal{H} = \frac{1}{2} \left[ g^{\alpha\beta} p_\alpha p_\beta + \omega_p^2 \left( 1 + \frac{g^2 B_0^2}{\omega_0^2 - \omega_\phi^2} \right) \right]. \quad (9)$$

The four velocity components for the photons in the equatorial plane ( $\theta = \pi/2$ ,  $p_\theta = 0$ ) are:

$$\dot{t} \equiv \frac{dt}{d\lambda} = \frac{-p_t}{f(r)}, \quad (10)$$

$$\dot{r} \equiv \frac{dr}{d\lambda} = p_r f(r), \quad (11)$$

$$\dot{\phi} \equiv \frac{d\phi}{d\lambda} = \frac{p_\phi}{r^2}, \quad (12)$$

where we have used the formula for obtaining four-velocity using the Hamiltonian,  $\dot{x}^\alpha = \partial \mathcal{H} / \partial p_\alpha$ . Using Eqs. (11) and (12), we can form a general equation for null trajectories

$$\frac{dr}{d\phi} = \frac{g^{rr} p_r}{g^{\phi\phi} p_\phi}. \quad (13)$$

The constraint equation  $\mathcal{H} = 0$ , sets the above equation as [18]

$$\frac{dr}{d\phi} = \sqrt{\frac{g^{rr}}{g^{\phi\phi}}} \sqrt{h^2(r) \frac{\omega_0^2}{p_\phi^2} - 1}, \quad (14)$$

where

$$h^2(r) \equiv -\frac{g^{tt}}{g^{\phi\phi}} - \frac{\omega_p^2}{g^{\phi\phi} \omega_0^2} \left( 1 + \frac{g^2 B_0^2}{\omega_0^2 - \omega_\phi^2} \right). \quad (15)$$

If we introduce the dimensionless parameters

$$\tilde{\omega}_\phi^2 = \frac{\omega_\phi^2}{\omega_0^2} \quad \text{and} \quad \tilde{B}^2 = \frac{g^2 B_0^2}{\omega_0^2}, \quad (16)$$

we can rewrite Eq. (15) for our non-commutative spacetime as

$$h^2(r) = r^2 \left[ \frac{\sqrt{\pi} r^2}{8\sqrt{\theta} - 2\sqrt{\pi} M r + \sqrt{\pi} r^2} - \frac{\omega_p^2(r)}{\omega_0^2} \left( 1 + \frac{\tilde{B}^2}{1 - \tilde{\omega}_\phi^2} \right) \right]. \quad (17)$$

where we have set  $g^{tt}$  and  $g^{\phi\phi}$  from Eq. (4). The photon sphere of radius  $r_{ph}$ , can be determined by solving the following equation [18]

$$\left. \frac{d(h^2(r))}{dr} \right|_{r=r_{ph}} = 0. \quad (18)$$

Now using Eq. (17) in (18) we can obtain a non-linear first order differential equation for the photon sphere radius  $r_{ph}$  for our non-commutative BH spacetime in the presence of axion-plasmon effects as:

$$\begin{aligned} & \frac{2 \left( \tilde{B}^2 - \tilde{\omega}_\phi^2 + 1 \right) \omega_p(r_{ph}) \left( r_{ph} \omega_p'(r_{ph}) + \omega_p(r_{ph}) \right)}{\omega_0^2 \left( \tilde{\omega}_\phi^2 - 1 \right)} \\ & + \frac{-6\pi M r_{ph}^3 + 32\sqrt{\pi} \sqrt{\theta} r_{ph}^2 + 2\pi r_{ph}^4}{\left( \sqrt{\pi} r_{ph} (2M - r_{ph}) - 8\sqrt{\theta} \right)^2} = 0 \end{aligned} \quad (19)$$

The roots of Eq. (19) cannot be obtained analytically because of its non-linearity and presence of mixed coupled terms as well as higher order terms in  $r_{ph}$ . Nevertheless, we can study it numerically by choosing different forms of  $\omega_p(r)$ .

Let us now calculate the angular shadow radius which can be defined with the help of the photon sphere radius  $r_{ph}$ . The angular shadow radius  $\alpha_{sh}$  is defined as:

$$\sin^2 \alpha_{sh} = \frac{h^2(r_{ph})}{h^2(r_o)} \quad (20)$$

Using Eq. (17), we can express Eq. (20) as

$$\sin \alpha_{sh} = \left[ \frac{r_{ph}^2 \left( \frac{\sqrt{\pi} r_{ph}^2}{8\sqrt{\theta} - 2\sqrt{\pi} M r_{ph} + \sqrt{\pi} r_{ph}^2} - \frac{\omega_p^2 \left( \frac{\tilde{B}^2}{1 - \tilde{\omega}_\phi^2} + 1 \right)}{\omega_0^2} \right)}{r_o^2 \left( \frac{\sqrt{\pi} r_o^2}{8\sqrt{\theta} - 2\sqrt{\pi} M r_o + \sqrt{\pi} r_o^2} - \frac{\omega_p^2 \left( \frac{\tilde{B}^2}{1 - \tilde{\omega}_\phi^2} + 1 \right)}{\omega_0^2} \right)} \right]^{1/2} \quad (21)$$

Here,  $r_{ph}$  and  $r_o$  denotes the photon sphere radius and observer's location respectively. If one assumes that the observer's location lies very far away from the BH, then the approximate BH shadow radius can be found by using Eq. (21) as follows: [47]

$$r_{sh} \approx r_o \sin \alpha_{sh}, \quad (22)$$

which gives

$$r_{sh} = r_{ph} \left[ \frac{\sqrt{\pi} r_{ph}^2}{8\sqrt{\theta} - 2\sqrt{\pi} M r_{ph} + \sqrt{\pi} r_{ph}^2} - \frac{\omega_p^2 \left( \frac{\tilde{B}^2}{1 - \tilde{\omega}_\phi^2} + 1 \right)}{\omega_0^2} \right]^{1/2} \quad (23)$$

Note that the shadow radius no longer depends on the observer's location. We can see that if one reconsiders the limiting case where there is no plasma medium,  $\omega_p \rightarrow 0$ , and where there is no contribution from the axionic and magnetic fields ( $\tilde{\omega}_\phi \rightarrow 0$  and  $\tilde{B} \rightarrow 0$  respectively), the trivial case of a Schwarzschild shadow radius ( $r_{sh}^{Sch} = 3\sqrt{3}M$ ) is obtained at  $r_{ph} = 3M$  (photon orbit radius for a Schwarzschild BH).

### III. PHOTON SPHERE RADIUS

In this section, we shall discuss how in the presence of a plasma medium, the effective motion of photons is affected due to the dispersive properties of the plasma. In this context, we shall adopt two specific cases. First, we assume a homogeneous plasma, which is characterized by a constant electron number density and plasma frequency, and hence a uniform refractive index. Secondly, we shall consider an inhomogeneous plasma, characterized by a power-law varying plasma frequency and hence a spatially varying refractive index. To be specific, we want to see how the photon radius depends on the particular nature of surrounding plasma medium.

#### A. Homogeneous Plasma

In case the non-commutative BH is surrounded by a homogeneous plasma characterized by a fixed plasma frequency i.e.  $\omega_p^2 = \text{const.}$ , the exact analytical expression for the radius of photon sphere from Eq. (19) can be hard to obtain. This is because, the surrounding plasma also constitutes the axionic field frequency  $\tilde{\omega}_\phi$  as well as a magnetic field  $\tilde{B}$ , coupled with the plasma frequency  $\omega_p$ , making them interdependent. Therefore, the photon sphere radius should be calculated numerically. In fact to be more specific, we shall plot the same with respect to the plasma frequency by setting different values of our three parameters of dependency, i.e the non-commutative parameter  $\theta$ , axion frequency  $\tilde{\omega}_\phi^2$  and the magnetic field  $\tilde{B}^2$ . For simplicity, we shall work with units where  $M = 1$ . The numerical results are plotted in Fig. 1. In the figure, we can see how the photon sphere radius varies with the plasma frequency, for any three values of the aforementioned model parameters. In Fig. 1 (a), for fixed values of  $\tilde{\omega}_\phi^2$  and magnetic field  $\tilde{B}^2$ , the photon sphere radius rises exponentially with the increase in plasma frequency  $\omega_p^2/\omega_0^2$ . One can see, the photon sphere radius starts with smaller values for larger values of  $\theta$ . This implies that as  $\theta$  increases, the shadow radius decreases. In Fig. 1 (b) and (c), however

we see a contrasting scenario with (a). In the former, keeping  $\theta = 0.02$  and  $\tilde{\omega}_\phi^2 = 0.5$ , we can see an exponential increase in photon sphere radius with increasing values of  $\omega_p^2/\omega_0^2$  for different values of  $\tilde{B}^2$  with  $\theta$  and  $\tilde{\omega}_\phi^2$  fixed, but for all cases the radius starts with the same value. This implies that, in the vacuum case  $\omega_p \rightarrow 0$ , there is no dependence of photon sphere radius with varying  $\tilde{B}^2$ . The slope of the curve however increases with increasing values of  $\tilde{B}^2$ . In the latter case, the same behaviour is apparent with the variation with the axion frequency  $\omega_\phi^2$ , while keeping  $\theta$  and  $\tilde{B}^2$  fixed. But, the slope of the curves vary moderately with changing values of axion frequency.

#### B. Inhomogeneous plasma with $\omega_p^2(r) = \kappa/r^q$

Next, let us investigate the dependence of an inhomogeneous plasma on the radii of photon spheres while including the axionic contribution. In this case, we may consider that plasma frequency as a radially dependent function following a power-law form as: [46, 48]

$$\omega_p^2(r) = \frac{\kappa}{r^q}. \quad (24)$$

In this context,  $\kappa$  and  $q$  are independent free parameters. The values of these parameters in the present work shall be fixed to  $q = 1$  and  $\kappa$  as a coupling constant [46]. The parameter  $q$  in fact quantifies how the intensity of plasma effect falls over radial distances. For instance, if one sets  $q = 2$ , the plasma frequency falls off like an inverse squared law and would signify a faster dilution of plasma effects as compared to  $q = 1$ . Therefore,  $q = 1$  case would provide a clearer impact of the presence of the plasma medium on the BH optical properties. Once again, we seek numerical solutions of the photon sphere radii by solving Eq. (19) for the case of inhomogeneous plasma. After solving Eq. (19), the photon sphere radii are plotted against the coupling constant of inhomogeneous plasma  $\kappa/\omega_0^2$ . From Fig. 2 (a), for a fixed value of  $\tilde{B}^2 = 0.3$  and  $\tilde{\omega}_\phi^2 = 0.5$  we can see that the variation of the photon sphere radius increases initially then tends to flatten out as the coupling constant  $\kappa/\omega_0^2$  increases. Also, as the non-commutative parameter decreases, the slope of the curve increases noticeably, signifying increase in value of  $r_{ph}$  as  $\theta$  decreases. Note that in the vacuum limit,  $\kappa \rightarrow 0$ , the photon sphere radius reduces to the same initial value, irrespective of the value of  $\theta$ . Next, in Figs. 2 (b) and (c), we see the same behaviour except in a way how the photon sphere radius vary with respect to changing  $\tilde{B}^2$  (see Fig. 2(b)). In other words, towards the vacuum limit, the photon sphere radius tends to have different initial values and these values increases with

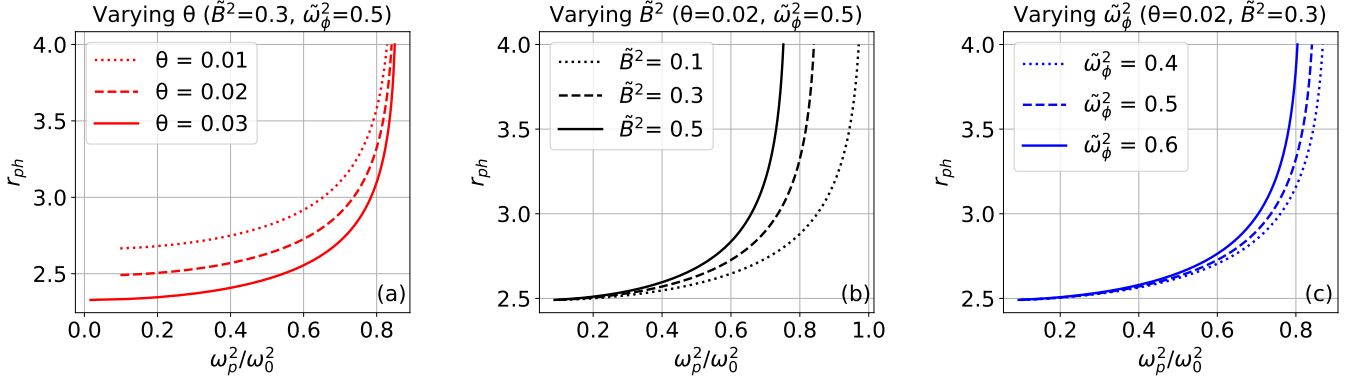


FIG. 1. Variation of photon sphere radius with the plasma frequency for various combinations of the parameters for a homogeneous plasma

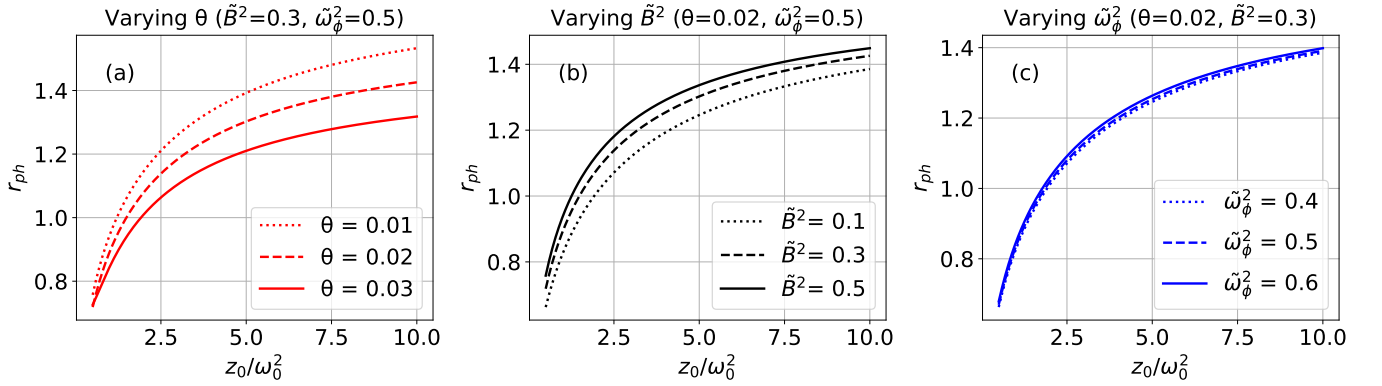


FIG. 2. Variation of photon sphere radius with the plasma frequency for various combinations of the parameters for an inhomogeneous plasma

increasing  $\tilde{B}^2$ . The overall slope of the curves has almost the same magnitude but with smaller deviations. In Fig. 2 (c), with respect to varying axion frequency  $\tilde{\omega}_\phi^2$ , the trend of variation of photon sphere radius is almost similar to the previous cases, but the effect of the axion field is minimal and no significant dependence on the slope of the curve is prominent here.

## IV. SHADOWS

### A. Homogeneous Plasma

Now let us discuss the behaviour of shadow cast by the non-commutative BH in the presence of plasma. To start with, we calculate the angular shadow through Eq.

(21). In homogeneous plasma case we can have:

$$\sin \alpha_{sh} = \left[ \frac{r_{ph}^2 \left( \frac{\sqrt{\pi} r_{ph}^2}{8\sqrt{\theta} - 2\sqrt{\pi} M r_{ph} + \sqrt{\pi} r_{ph}^2} - \frac{\omega_p^2 \left( \frac{\tilde{B}^2}{1 - \tilde{\omega}_\phi^2} + 1 \right)}{\omega_0^2} \right)}{r_o^2 \left( \frac{\sqrt{\pi} r_o^2}{8\sqrt{\theta} - 2\sqrt{\pi} M r_o + \sqrt{\pi} r_o^2} - \frac{\omega_p^2 \left( \frac{\tilde{B}^2}{1 - \tilde{\omega}_\phi^2} + 1 \right)}{\omega_0^2} \right)} \right]^{1/2} \quad (25)$$

where  $\omega_p$  is treated as a constant. Fig. 3 shows the numerical plot of the angular shadow with respect to observer's position. In Fig. 3(a), the axion frequency  $\tilde{\omega}_\phi$  and  $\tilde{B}^2$  are kept fixed at 0.5 and 0.3, respectively, while the constant homogeneous plasma frequency is set to  $\omega_p = 0.5$ . We have solved for the photon sphere radius  $r_{ph}$  from the condition (19), for each case and used those in Eq. (25). It is seen that the angular shadow  $\alpha_{sh}$  decreases asymptotically with increasing observer distance, with the variation noticeably influenced by the non-commutative parameter  $\theta$ . As  $\theta$  increases, the angular shadow starts from smaller values, while the slope

of the curves remains unchanged. Figs. 3(b) and (c) also exhibits analogous behavior. In Fig. 3(b), the dependence of the angular shadow on the axion frequency is relatively weak provided  $\theta = 0.02$ ,  $\tilde{B}^2 = 0.3$ , and  $\omega_p = 0.5$  are held constant. In Fig. 3(c), under the conditions  $\theta = 0.02$ ,  $\tilde{\omega}_\phi^2 = 0.3$ , and  $\omega_p = 0.5$ , the angular shadow continues to decrease with observer distance, yet it tends to converge to similar values for observers positioned at nearer regions of the BH.

The shadow radius can be calculated from Eq. (23) as

$$r_{sh} = r_{ph} \left[ \frac{\sqrt{\pi} r_{ph}^2}{8\sqrt{\theta} - 2\sqrt{\pi} M r_{ph} + \sqrt{\pi} r_{ph}^2} - \frac{\omega_p^2 \left( \frac{\tilde{B}^2}{1 - \tilde{\omega}_\phi^2} + 1 \right)}{\omega_0^2} \right]^{1/2} \quad (26)$$

The expression remains same as that of Eq. (23) except here  $\omega_p^2$  is a constant. Using Eq. (26), we plotted of the shadows of the BH in the Cartesian plane, as shown in Fig. 5. In Fig. 5(a), it is clear that the non-commutative parameter  $\theta$ , while having fixed values for  $\tilde{\omega}_\phi^2$  and  $\tilde{B}^2$  and setting  $\omega_p$  to 0.5, clearly influences the shadow size. In particular, an increase in  $\theta$  results in a smaller shadow. A similar effect is observed while varying  $\tilde{B}^2$ , where an increase in the magnetic field causes an expansion in the shadow radius, as can be seen from Fig. 5(c). In contrast, changes in  $\tilde{\omega}_\phi^2$  have a very minimal effect on the size of the shadows, as is observed from Fig. 5(b).

## B. Inhomogeneous Plasma

Next, in the inhomogeneous plasma case setting  $\omega_p^2 = \kappa/r^q$ , where  $q = 1$  in Eq. (21) we can obtain the angular shadow as:

$$\sin \alpha_{sh} = \left[ \frac{r_{ph}^2 \left( \frac{\sqrt{\pi} r_{ph}^2}{8\sqrt{\theta} - 2\sqrt{\pi} M r_{ph} + \sqrt{\pi} r_{ph}^2} - \frac{\kappa^2 \left( \frac{\tilde{B}^2}{1 - \tilde{\omega}_\phi^2} + 1 \right)}{\omega_0^2 r_{ph}^2} \right)}{r_o^2 \left( \frac{\sqrt{\pi} r_o^2}{8\sqrt{\theta} - 2\sqrt{\pi} M r_o + \sqrt{\pi} r_o^2} - \frac{\kappa^2 \left( \frac{\tilde{B}^2}{1 - \tilde{\omega}_\phi^2} + 1 \right)}{\omega_0^2 r_o^2} \right)} \right]^{1/2} \quad (27)$$

Eq. (27) is analyzed by plotting for various combinations of the parameters, like we did in the previous subsection for the homogeneous plasma case. The key distinction in this analysis lies in the inclusion of the inhomogeneous plasma coupling parameter,  $\kappa$ . For the purposes of this work, we have adopted a constant value of  $\kappa = 0.5$ , though it is important to note that  $\kappa$  may assume any arbitrary positive values in general. Fig. 4(a) shows the variation of the angular shadow as a function of the observer's position, for several different values of the non-commutative parameter  $\theta$ . In this case, we

have set  $\tilde{\omega}_\phi^2 = 0.5$  and  $\tilde{B}^2 = 0.3$ . It is observed that the angular shadow decreases as the observer moves farther from the black hole. Notably, the dependence on  $\theta$  becomes evident: as the observer approaches the black hole, the angular shadow tends to increase for smaller values of the non-commutative parameter  $\theta$ . In Fig. 4(b), the variation of the angular shadow is shown for different values of the axion frequency  $\tilde{\omega}_\phi^2$ , while maintaining fixed values for  $\theta$  and  $\tilde{B}^2$ . The overall trend is qualitatively similar to the previous cases, with a very feeble dependence on the axion frequency. A similar observation can be made when considering the dependence on varying  $\tilde{B}^2$  values, as displayed in Fig. 4(c). From these analyses, it is clear that neither the axion frequency  $\tilde{\omega}_\phi^2$  nor the magnetic field  $\tilde{B}^2$  exerts a significant influence on the angular shadow within the context of an inhomogeneous plasma. These results points towards the conclusion that the primary factor influencing the angular shadow in this scenario is the observer's position, with only noticeable effects arising from variations in the non-commutative parameter  $\theta$ . The dependence on the axion frequency and magnetic field however is quite subtle in the case of inhomogeneous plasma. This is one of the important result of this analysis.

The shadow radius in the case of inhomogeneous plasma can be calculated from Eq. (23) as

$$r_{sh} = r_{ph} \left[ \frac{\sqrt{\pi} r_{ph}^2}{8\sqrt{\theta} - 2\sqrt{\pi} M r_{ph} + \sqrt{\pi} r_{ph}^2} - \frac{\kappa^2 \left( \frac{\tilde{B}^2}{1 - \tilde{\omega}_\phi^2} + 1 \right)}{\omega_0^2 r_{ph}^2} \right]^{1/2} \quad (28)$$

Using Equation (28), we have generated a plot of the shadows in the Cartesian plane, as portrayed in Fig. 6. In Fig. 6(a), it is evident that the non-commutative parameter  $\theta$ , while maintaining fixed values of  $\tilde{\omega}_\phi^2$  and  $\tilde{B}^2$  and setting  $\kappa$  to 0.5, uniquely influences the size of the shadows. Consistent with the results in the homogeneous plasma scenario in subsection IV A, an increase in the non-commutative parameter leads to a reduction in shadow size. Furthermore, Figs. 6(b) and (c) exhibits a subtle dependence on the variations of  $\tilde{\omega}_\phi^2$  and  $\tilde{B}^2$ , respectively. A closer look at the zoomed in figures of (b) and (c) reveals that an increase in  $\tilde{\omega}_\phi^2$  leads to a decrease in the shadow radius, and similarly, an increase in  $\tilde{B}^2$  also results in a smaller shadow radius.

## V. OBSERVATIONAL CONSTRAINTS

In the strong-gravity regime, the EHT's most recent horizon-scale image of Sgr A\* [49] offers an ideal platform to test theories of gravity and fundamental

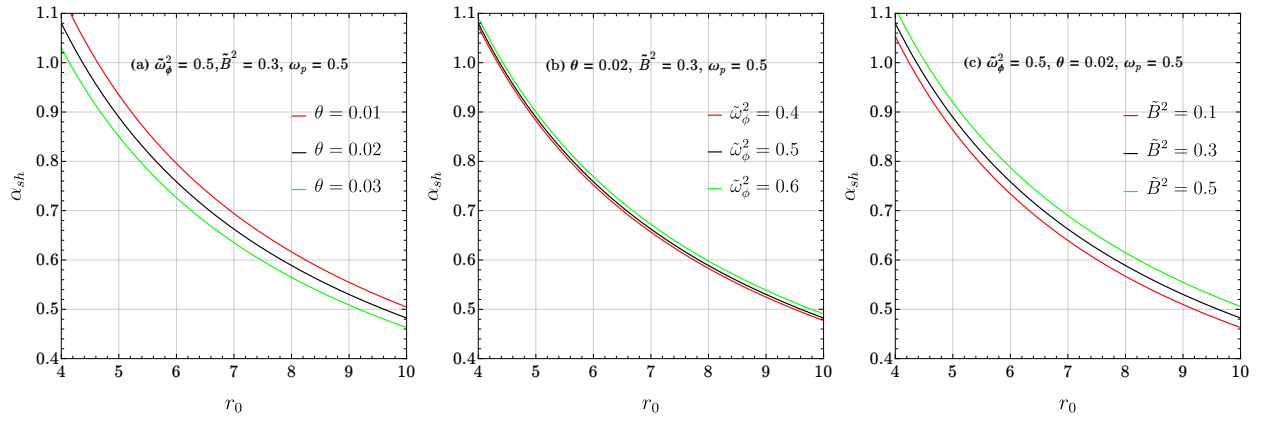


FIG. 3. Variation of angular shadow with the observer's position for various combinations of the parameters for a homogeneous plasma

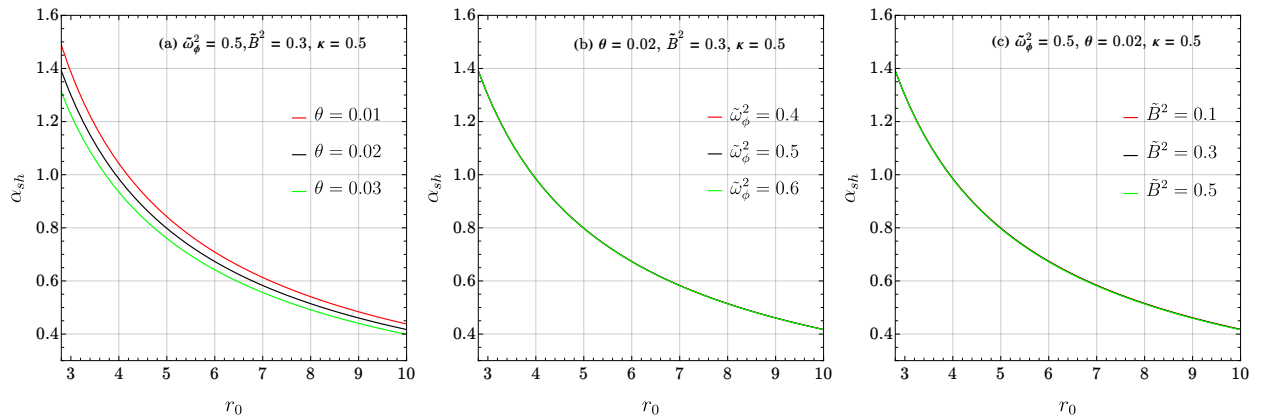


FIG. 4. Variation of angular shadow with the observer's position for various combinations of the parameters for an inhomogeneous plasma

physics. Because Sgr A\* is so very near to us, estimating its mass, distance, and, consequently, its mass-to-distance ratio, becomes very much easier. Compared to M87\*, whose mass is not strictly restricted by the stellar dynamics observations, this poses itself as a significant benefit. The mass of the Sgr A\* ( $O(10^6)M_\odot$ ) is much smaller than that of the M87\* ( $O(10^9)M_\odot$ ), opening up a whole new way of looking at fundamental physics in the strong curvature regime. The Sgr A's shadow can also offer more rigorous limits on fundamental parameters than the M87's, using the same reasoning [50].

The EHT has determined the fractional deviation between the predicted shadow radius  $r_s$  and the shadow radius of a Schwarzschild BH  $r_{sch} = 3\sqrt{3}M$ , given by:

$$\delta \equiv \frac{r_s}{r_{sch}} - 1 = \frac{r_s}{3\sqrt{3}M} - 1. \quad (29)$$

The Keck and VLTI set the following constraints on  $\delta$  as:

[50–52]

$$\delta = -0.04_{-0.10}^{+0.09} \text{ (Keck)} \quad \text{and} \quad \delta = -0.08_{-0.09}^{+0.09} \text{ (VLTI)}$$

For a convenient analysis, we may calculate the average value of  $\delta$  estimated from the Keck and VLTI observations since these values are uncorrelated as they are originated from independent measurements. Thus the average value of  $\delta$  is

$$\delta \approx -0.060 \pm 0.065. \quad (30)$$

If one assumes a Gaussian posterior distribution, the confidence intervals for  $\delta$  are

$$-0.125 \lesssim \delta \lesssim 0.005 \quad (1\sigma) \quad \text{and} \quad -0.19 \lesssim \delta \lesssim 0.07 \quad (2\sigma). \quad (31)$$

Extracting  $r_s$  from Eq. (29), we get

$$\frac{r_s}{M} = 3\sqrt{3}(\delta + 1), \quad (32)$$



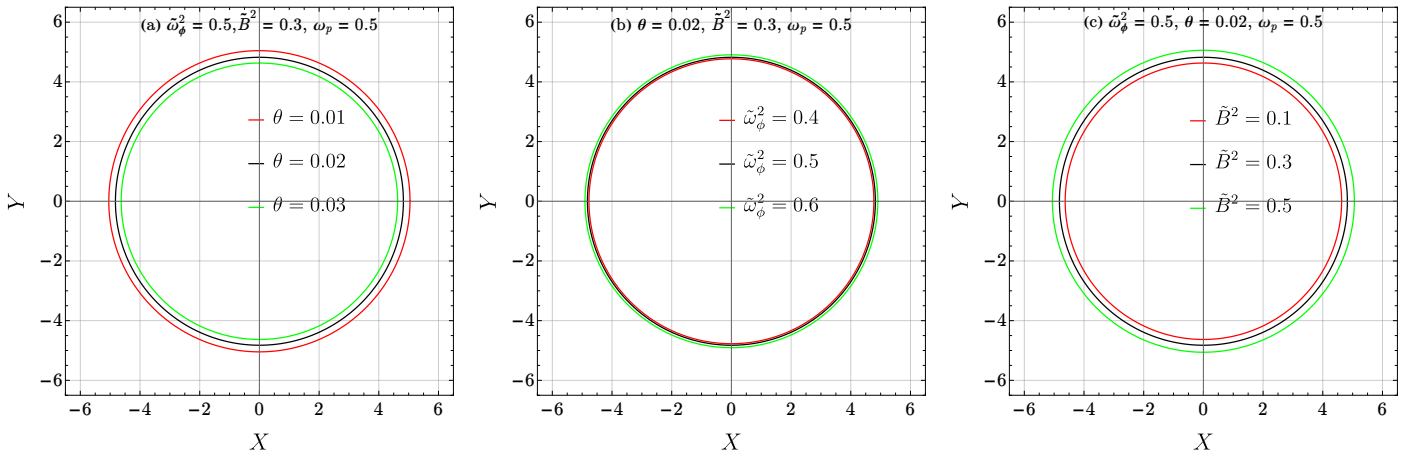


FIG. 5. Shadow images for various combinations of the parameters for a homogeneous plasma

which when combined with the constraints Eq. (31), gives

$$4.55 \lesssim r_s/M \lesssim 5.22, (1\sigma) \text{ and } 4.21 \lesssim r_s/M \lesssim 5.56, (2\sigma). \quad (33)$$

To examine the shadow constraints on our model parameters, we use Eqs. (26) and (28) and plot it in comparison to the observational data as mentioned above. The Tab. I shows the obtained constraints on the pa-

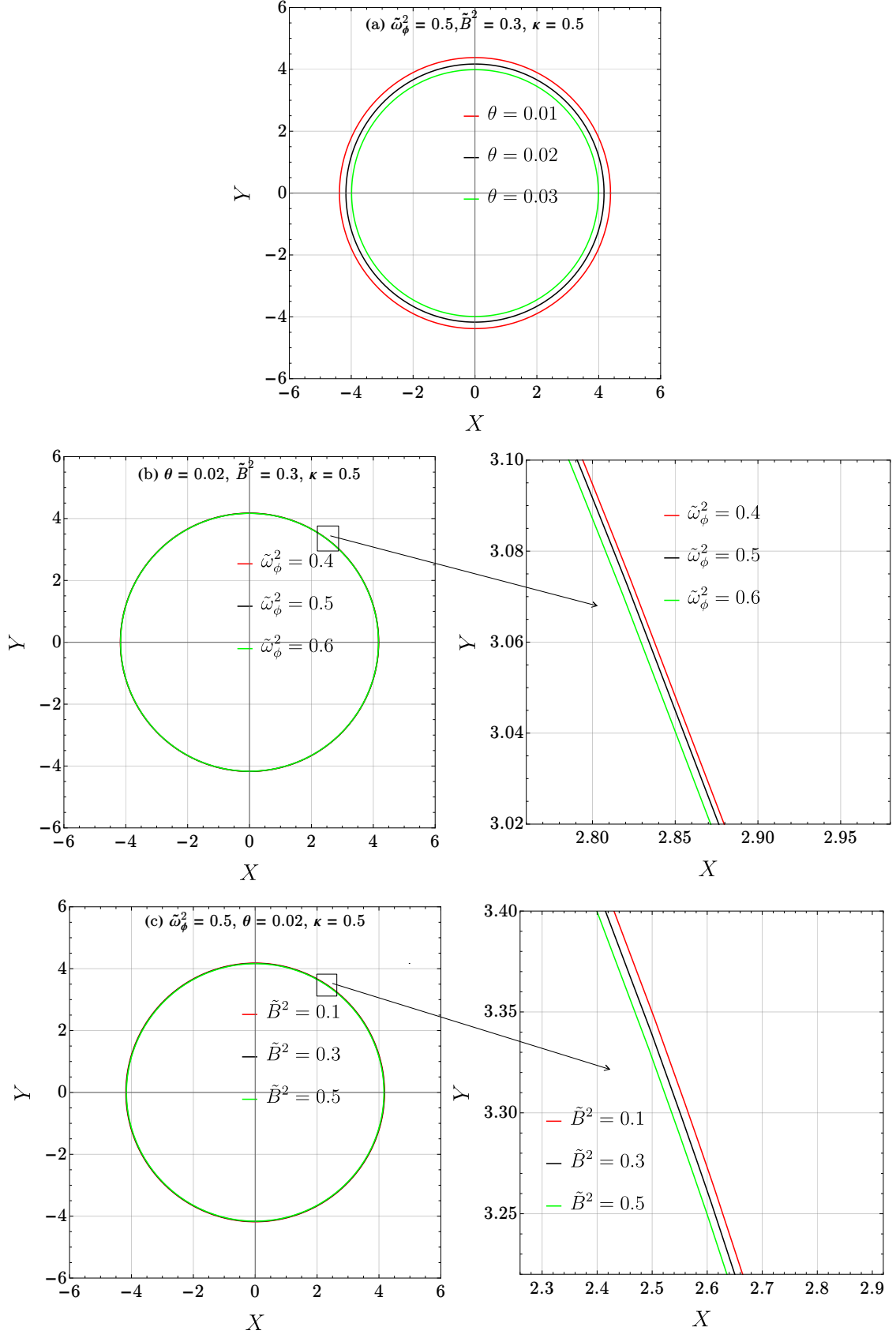
rameters with respect to the Sgr\* shadow data. We note that for both homogeneous and inhomogeneous plasma cases, the non-commutative parameter  $\theta$  is very tightly constrained on both  $1\sigma$  and  $2\sigma$  confidence levels. Moreover, the axion frequency  $\tilde{\omega}_\phi$  is not constrained at  $1\sigma$  level for both types of plasma. Also, the magnetic field parameter  $\tilde{B}^2$  remains unconstrained at the  $1\sigma$  confidence level.

- 
- [1] P. Nicolini, NONCOMMUTATIVE BLACK HOLES, THE FINAL APPEAL TO QUANTUM GRAVITY: A REVIEW, *Int. J. Mod. Phys. A* **24**, 1229 (2009).
- [2] M. Schneider and A. DeBenedictis, Noncommutative black holes of various genera in the connection formalism, *Phys. Rev. D* **102**, 024030 (2020).
- [3] C. Bastos, O. Bertolami, N. C. Dias, *et al.*, Noncommutative black holes, *J. Phys. Conf. Ser.* **222**, 012033 (2010).
- [4] T. Toghray, A. E. L. Boukili, N. Mansour, *et al.*, Noncommutative formulation of Schwarzschild black hole and its physical properties, *Indian J. Phys.* **97**, 4497 (2023).
- [5] P. Bhar, D. J. Gogoi, and S. Ponglertsakul, Noncommutative black hole in de Rham-Gabadadze-Tolley like massive gravity, *Ann. Phys.* **475**, 169951 (2025).
- [6] M. A. S. Afshar and J. Sadeghi, Mutual influence of photon sphere and non-commutative parameter in various non-commutative black holes: Towards evidence for WGC, *Phys. Dark Universe* **47**, 101814 (2025).
- [7] M. A. S. Afshar and J. Sadeghi, WGC as WCCC protector: The synergistic effects of various parameters in non-commutative black holes for identifying WGC candidate models, *Nucl. Phys. B* **1014**, 116872 (2025).
- [8] R.-B. Wang, S.-J. Ma, L. You, *et al.*, Thermodynamics of Schwarzschild-AdS black hole in non-commutative geometry, *Chin. Phys. C* **10.1088/1674-1137/adbacd** (2025).
- [9] H. Quevedo and M. N. Quevedo, Quasi-Homogeneous Black Hole Thermodynamics in Non-Commutative Geometry, *Universe* **11**, 79 (2025).
- [10] B. Tan, Thermodynamics of high order correction for Schwarzschild-AdS black hole in non-commutative geometry, *Nucl. Phys. B* **1014**, 116868 (2025).
- [11] A. A. A. Filho, N. Heidari, and A. Övgün, Axisymmetric black hole in a non-commutative gauge theory: classical and quantum gravity effects, *arXiv* **10.48550/arXiv.2502.12039** (2025), 2502.12039.
- [12] A. A. Araújo Filho, J. R. Nascimento, A. Yu. Petrov, *et al.*, Properties of an axisymmetric Lorentzian non-commutative black hole, *Phys. Dark Universe* **47**, 101796 (2025).
- [13] A. Bahroz Brzo, S. N. Gashti, B. Pourhassan, *et al.*, Thermodynamic topology of AdS black holes within non-commutative geometry and Barrow entropy, *Nucl. Phys. B* **1012**, 116840 (2025).
- [14] A. Ashraf, T. Naseer, H. Chaudhary, *et al.*, Observational constraints on QPOs with orbital motion around charged non-commutative Schwarzschild black hole surrounded by perfect fluid dark matter, *Nucl. Phys. B* **1014**, 116873 (2025).
- [15] R.-B. Wang, L. You, S.-J. Ma, *et al.*, Thermodynamic properties and Joule-Thomson expansion of AdS black hole

Homogeneous Plasma			Inhomogeneous Plasma		
Parameter	$1\sigma$	$2\sigma$	Parameter	$1\sigma$	$2\sigma$
$\theta$	$0 < \theta \leq 0.01448$	$0 < \theta \leq 0.0322$	$\theta$	$0.02750 < \theta \leq 0.05881$	$0.0122 < \theta \leq 0.06$
$\tilde{\omega}_\phi^2$	--	$0 < \tilde{\omega}_\phi^2 \leq 0.942$	$\tilde{\omega}_\phi^2$	--	$0 < \tilde{\omega}_\phi^2 \leq 0.6262$
$\tilde{B}^2$	--	$0 < \tilde{B}^2 < 0.4788$	$\tilde{B}^2$	$0 < \tilde{B}^2 < 0.2402$	$0 < \tilde{B}^2 < 0.4738$

TABLE I. The constraints on the model parameters at  $1\sigma$  and  $2\sigma$  confidence intervals with respect to the Sgr\* shadow data.

- with Gaussian distribution in non-commutative geometry, arXiv [10.48550/arXiv.2503.12363](https://arxiv.org/abs/10.48550/arXiv.2503.12363) (2025), [2503.12363](https://arxiv.org/abs/2503.12363).
- [16] B. Hamil and B. C. Lütffüoğlu, Phantom RN-AdS black holes in noncommutative space, *Eur. Phys. J. C* **85**, 1 (2025).
- [17] F. Atamurotov, B. Ahmedov, and A. Abdujabbarov, Optical properties of black holes in the presence of a plasma: The shadow, *Phys. Rev. D* **92**, 084005 (2015).
- [18] V. Perlick, O. Yu. Tsupko, and G. S. Bisnovaty-Kogan, Influence of a plasma on the shadow of a spherically symmetric black hole, *Phys. Rev. D* **92**, 104031 (2015).
- [19] A. Abdujabbarov, B. Toshmatov, Z. Stuchlík, *et al.*, Shadow of the rotating black hole with quintessential energy in the presence of the plasma, arXiv [10.48550/arXiv.1512.05206](https://arxiv.org/abs/10.48550/arXiv.1512.05206) (2015), [1512.05206](https://arxiv.org/abs/1512.05206).
- [20] Y. Huang, Y.-P. Dong, and D.-J. Liu, Revisiting the shadow of a black hole in the presence of a plasma, *Int. J. Mod. Phys. D* **27**, 1850114 (2018).
- [21] A. Chowdhuri and A. Bhattacharyya, Shadow analysis for rotating black holes in the presence of plasma for an expanding universe, *Phys. Rev. D* **104**, 064039 (2021).
- [22] H.-M. Wang and S.-W. Wei, Shadow cast by Kerr-like black hole in the presence of plasma in Einstein-bumblebee gravity, arXiv [10.48550/arXiv.2106.14602](https://arxiv.org/abs/10.48550/arXiv.2106.14602) (2021), [2106.14602](https://arxiv.org/abs/2106.14602).
- [23] J. Badía and E. F. Eiroa, Shadow of black holes with a plasma environment in 4D Einstein-Gauss-Bonnet gravity (2022) pp. 3856–3864.
- [24] A. Arvanitaki and S. Dubovsky, Exploring the string axiverse with precision black hole physics, *Phys. Rev. D* **83**, 044026 (2011).
- [25] A. Arvanitaki, M. Baryakhtar, and X. Huang, Discovering the QCD axion with black holes and gravitational waves, *Phys. Rev. D* **91**, 084011 (2015).
- [26] A. B. Balakin, R. K. Muharlamov, and A. E. Zayats, Electromagnetic waves in an axion-active relativistic plasma non-minimally coupled to gravity, *Eur. Phys. J. C* **73**, 1 (2013).
- [27] M. Lyutikov, Production of axions during scattering of Alfvén waves by fast-moving Schwarzschild black holes, arXiv [10.48550/arXiv.2108.06364](https://arxiv.org/abs/10.48550/arXiv.2108.06364) (2021), [2108.06364](https://arxiv.org/abs/2108.06364).
- [28] S. Sen, Plasma effects on lasing of a uniform ultralight axion condensate, *Phys. Rev. D* **98**, 103012 (2018).
- [29] H. Terças, J. D. Rodrigues, and J. T. Mendonça, Axion-Plasmon Polaritons in Strongly Magnetized Plasmas, *Phys. Rev. Lett.* **120**, 181803 (2018).
- [30] F. Atamurotov, K. Jusufi, M. Jamil, *et al.*, Axion-plasmon or magnetized plasma effect on an observable shadow and gravitational lensing of a Schwarzschild black hole, *Phys. Rev. D* **104**, 064053 (2021).
- [31] M. Khodadi, Shadow of black hole surrounded by magnetized plasma: Axion-plasmon cloud, *Nucl. Phys. B* **985**, 116014 (2022).
- [32] Y. Pahlavon, F. Atamurotov, K. Jusufi, *et al.*, Effect of magnetized plasma on shadow and gravitational lensing of a Reissner–Nordström black hole, *Phys. Dark. Univ.* **45**, 101543 (2024).
- [33] R. Ali, X. Tiecheng, M. Awais, *et al.*, Study of light deflection and shadow from a hairy black hole under the influence of the non-magnetic plasma, *Chin. J. Phys.* **94**, 416 (2025).
- [34] R. V P and S. R, Strong Gravitational Lensing and Shadows by Quantum Schwarzschild Black Hole in Homogeneous Plasma, *Int. J. Theor. Phys.* **64**, 1 (2025).
- [35] D. Umarov, O. Yunusov, F. Atamurotov, *et al.*, Plasma effects on weak gravitational lensing and shadows of Sen black holes\*, *Chin. Phys. C* **49**, 055102 (2025).
- [36] A. Alimova, Z. Turakhonov, F. Atamurotov, *et al.*, Shadow and weak gravitational lensing of RN-like BH in plasma, *Phys. Dark. Univ.* **47**, 101749 (2025).
- [37] T. Ibrokhimov, Z. Turakhonov, F. Atamurotov, *et al.*, Testing regular scale-dependent black hole space time using particle dynamics: Shadow and gravitational weak lensing, *Phys. Dark. Univ.* **47**, 101778 (2025).
- [38] Z. Turakhonov, F. Atamurotov, S. G. Ghosh, *et al.*, Probing effects of plasma on shadow and weak gravitational lensing by regular black holes in asymptotically safe gravity, *Phys. Dark Universe* **48**, 101880 (2025).
- [39] F. Mushtaq, M. Yasir, and X. Tiecheng, Particle motion and lensing with plasma of black hole in coincident gravity coupled to nonlinear electrodynamics, *Eur. Phys. J. Plus* **140**, 1 (2025).
- [40] M. Alloqulov, Y. Isaqjonov, S. Shaymatov, *et al.*, Shadow and gravitational weak lensing around a quantum-corrected black hole surrounded by plasma\*, *Chin. Phys. C* **49**, 045104 (2025).
- [41] S. Yasmeen, K. Jafarzade, and M. Jamil, Shadow Cast by the Kerr MOG Black Hole under the Influence of Plasma and Constraints from EHT Observation, *Chin. Phys. C* [10.1088/1674-1137/adb9c5](https://doi.org/10.1088/1674-1137/adb9c5) (2025).
- [42] R. Ali, X. Tiecheng, R. Babar, *et al.*, Exploring Light Deflection and Black Hole Shadows in Rastall Theory with



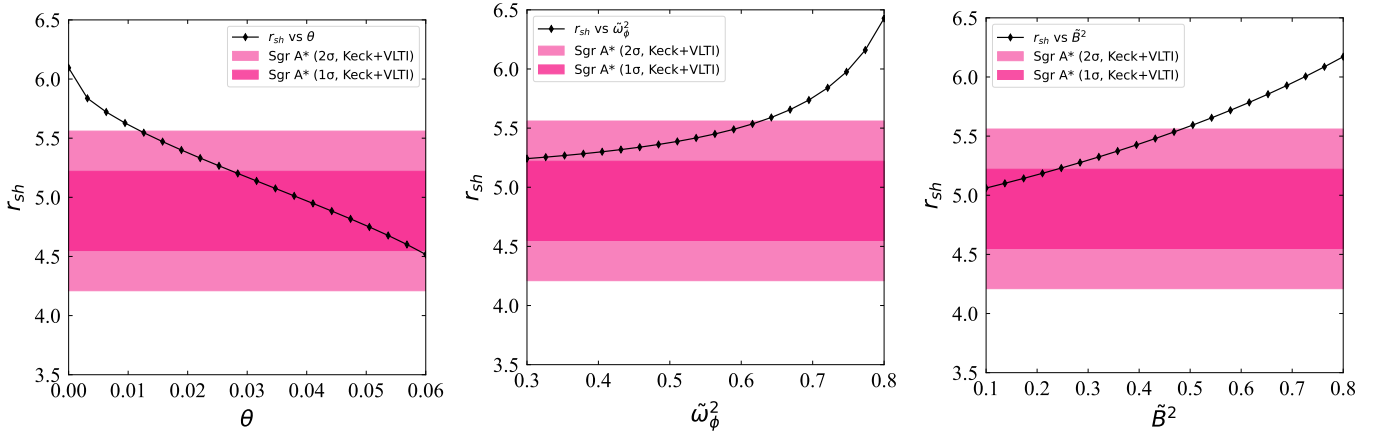


FIG. 7. Variation of shadow radius with the model parameters for homogeneous plasma case with respect to the observational data. Here we have set  $\omega_0^2 = 1$ ,  $\tilde{\omega}_\phi^2 = 0.5$  and  $\tilde{B}^2 = 0.3$ . Here we have set the observer at  $r_o = 75$ .

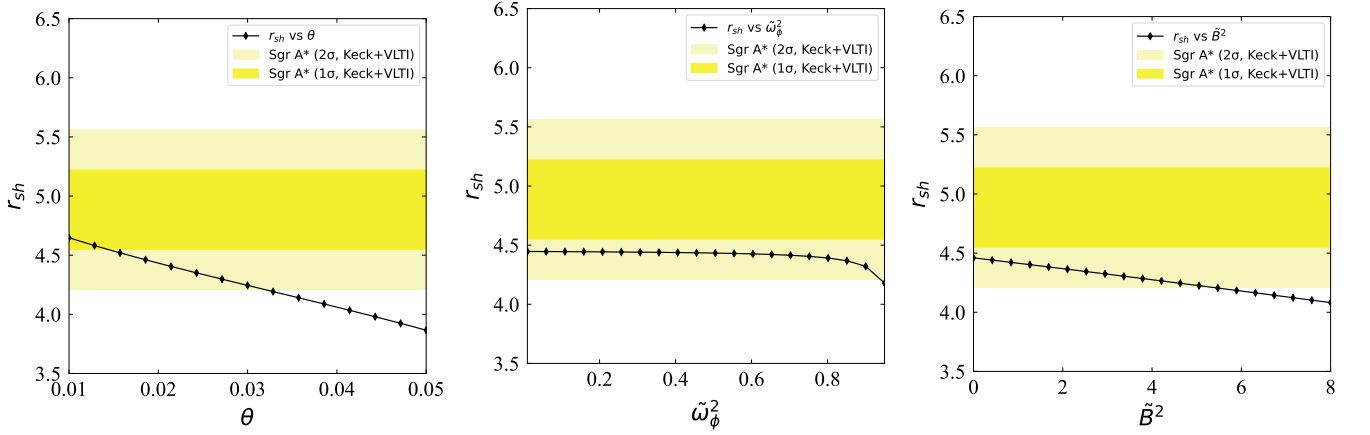


FIG. 8. Variation of shadow radius with the model parameters for inhomogeneous plasma case with respect to the observational data. Here we have set  $\omega_0^2 = 1$ ,  $\kappa^2 = 0.5$ . Here we have set the observer at  $r_o = 75$ .

Plasma Effects, *Int. J. Theor. Phys.* **64**, 1 (2025).

- [43] J. T. Mendonça, J. D. Rodrigues, and H. Terças, Axion production in unstable magnetized plasmas, *Phys. Rev. D* **101**, 051701 (2020).
- [44] F. Wilczek, Two applications of axion electrodynamics, *Phys. Rev. Lett.* **58**, 1799 (1987).
- [45] J. L. Synge, *Relativity: The General Theory*. North-Holland, Amsterdam, 1960.
- [46] A. Rogers, Frequency-dependent effects of gravitational lensing within plasma, *Mon. Not. R. Astron. Soc.* **451**, 17 (2015).
- [47] V. Perlick and O. Yu. Tsupko, Calculating black hole shadows: Review of analytical studies, *Phys. Rep.* **947**, 1 (2022).
- [48] X. Er and A. Rogers, Two families of astrophysical diverging lens models, *Mon. Not. R. Astron. Soc.* **475**, 867 (2018), arXiv:1712.06900.
- [49] Event Horizon Telescope Collaboration, K. Akiyama, A. Alberdi, *et al.*, First Sagittarius A\* Event Horizon Telescope Results. I. The Shadow of the Supermassive Black Hole in the Center of the Milky Way, *Astrophys. J. Lett.* **930**, L12 (2022).
- [50] S. Vagnozzi, R. Roy, Y.-D. Tsai, *et al.*, Horizon-scale tests of gravity theories and fundamental physics from the Event Horizon Telescope image of Sagittarius A\*, *Classical Quantum Gravity* **40**, 165007 (2023).
- [51] T. Do, A. Hees, A. Ghez, *et al.*, Relativistic redshift of the star S0-2 orbiting the Galactic Center supermassive black hole, *Science* **365**, 664 (2019).
- [52] R. Abuter, A. Amorim, M. Bauböck, *et al.*, Detection of the Schwarzschild precession in the orbit of the star S2 near the Galactic centre massive black hole, *Astron. Astrophys.* **636**, L5 (2020).